ORIGINAL PAPER

One-step hydrothermal synthesis of reduced graphene oxide/carbon nanotubes/hydroquinone hydrogel and its electrochemical properties

Kelei Wang[1] · **Lei Hua**[1] · **Zhongbing Wang**[1] · **Chunnian Chen**[1]

Abstract

Using oxalic acid as a reducing agent, hydroquinone (HQ), graphene (GO), and acidified carbon nanotubes (CNTs) were compounded directly to synthesize reduced graphene oxide (rGO)/CNTs/HQ hydrogels by a one-step hydrothermal method, and the phase composition and electrochemical properties were studied. During the hydrothermal reaction, the π bond in the hydroquinone molecule will be compounded with the large π bond on the surface of rGO due to the π-π interaction. At the same time, CNTs play a role of spacer and support in rGO/CNTs/HQ and improve the conductivity of rGO/CNTs/HQ. The prepared rGO/CNTs/HQ has a mass-specific capacitance of 219 Fg^{-1} at 0.5 Ag^{-1}; at 10 Ag^{-1}, the mass-specific capacitance retains 81%, confirming its excellent rate performance; After 2000 cycles, the mass ratio capacitance retains 94%, and the cycle performance is excellent.

Keywords Hydroquinone · Graphene · Carbon nanotubes · Hydrogel · Nanocomposite

Introduction

The storage of fossil energy in the world is fixed, and with the consumption of resources, the energy crisis continues to intensify. New energy is a key issue that needs to be solved urgently, and there is an urgent need for the emergence of green and environmentally friendly new energy. Supercapacitors have gained more and more attention in recent years due to the advantages of fast charging and discharging speed and excellent cycle performance [1–4]. Wu X et al. prepared P-doped porous carbon nanosheet confined Te nanocrystals as a highly stable electrode material for the battery-supercapacitor hybrid system. When the composite material is used as a cathode material, it can exhibit a specific capacity of 153 $mAhg^{-1}$. As an anode material, the composite material exhibits a specific capacitance of 263 Fg^{-1}. In addition, the composite material can be stably cycled more than 10,000 times in the KOH electrolyte [5].Graphene can be understood as GO without oxygen-containing functional groups on the sheet. Graphene has excellent electrochemical properties and has been the focus of scientific research since its inception. Ling-Li Xing et al. prepared three-dimensional (3D) flower-shaped $Li_4Ti_5O_{12}$-graphene (Gr) hybrid micro/nano structures and pine needle-derived carbon nanopores (PNDCN) by using an effective hydrothermal process. The obtained 3D $Li_4Ti_5O_{12}$-Gr shows a high specific capacitance of 706.52 Fg^{-1} at 1 Ag^{-1}. The prepared PNDCN also showed a high specific capacitance of 314.50 Fg^{-1} at 1 Ag^{-1} [6]. Wu X et al. prepared ultra-fine metallic VSe_2 nanoparticles anchored reduced graphene oxide composite by one-step hydrothermal method. The composite material has a high specific capacity of 156.8 $mAhg^{-1}$ at 1 Ag^{-1}. This study clarifies that metal VSe_2 can be used in high-performance energy storage cathode materials [7]. In addition, graphene has also achieved excellent research results in compounding with metal oxides [8], metal hydroxides [9], metal organic frameworks [10–13], and modification with metal elements [14].

Carbon nanotubes are very light carbon materials. It has a special tubular structure and excellent conductivity at the same time. When used as a good medium in combination with other materials, it can improve the conductivity of the material and increase the transfer speed of charges. Due to

✉ Chunnian Chen
   chencn@hfut.edu.cn

1   Anhui Province Key Laboratory of Advance Catalytic
    Material and Reaction Engineering, Anhui Province
    Key Laboratory of Green Manufacturing of Power
    Battery, School of Chemistry and Chemical Engineering,
    Hefei University of Technology, Hefei 230009,
    People's Republic of China

its unique size effect, carbon nanotubes can form a conductive network with numerous conductive paths [15, 16].

As mentioned earlier, graphene has been widely used due to its excellent properties and has also been reflected as an electrode material [17]. Hydrogels and aerogels are two specific application examples of such three-dimensional macroscopic assemblies with high specific surface area. Because their microporous and mesoporous interconnection networks allow the entry and diffusion of ions and molecules, they are used in electrode materials, Catalysis and water treatment have attractive potential [18, 19]. Due to the three-dimensional network structure of the hydrogel, the hydrogel has a good ability to embed materials, thereby significantly improving its physical properties [20]. Due to the unique properties of carbon nanotubes, some researchers have prepared them into hydrogel composite materials to play their advantages [21]. However, the application of carbon nanotubes is limited by their poor solubility in water, and the use of surfactants or polymers to aid dispersion will reduce their unique properties. There are many oxygen functional groups on graphene oxide, and the oxygen-containing functional groups carried on the edge of the sheet allow graphene oxide to chemically react with other materials [22]. Graphene oxide can also effectively disperse carbon nanotubes through the mutual accumulation of π-π chemical bonds [23, 24]. Recently, the combined use of carbon nanotubes and graphene has been used in practical applications in industrial production, including lithium-ion batteries [25], heavy metal removal [26], and petroleum adsorption [27]. The core process of preparing a well-structured graphene hydrogel is to make the graphene oxide-based suspension into a gel through chemical reduction [28].

Hydroquinone, p-aminophenol, acenaphthylene quinone, and other small organic molecules can also be used as electrode materials in supercapacitors due to their special structure. The functional groups they carry can undergo Faraday reactions to provide pseudocapacitances. When they are combined with carbon materials such as mesoporous carbon [29] and graphene [30, 31], they can have the advantages of both electric double layer capacitors and pseudocapacitors. Under the synergistic effect, it will have excellent electrochemical performance.

As an excellent organic electrochemical reaction medium, hydroquinone (HQ) has begun to be used in the field of energy storage. Because the oxygen-containing functional group contained in hydroquinone can be transformed into a quinone structure during charge and discharge, it can produce an ideal pseudocapacitance [32]. The oxygen-containing functional groups contained in hydroquinone can undergo the following reactions during the electrochemical reaction:
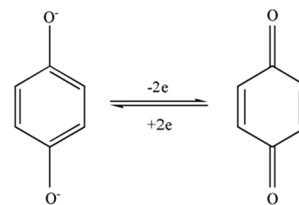
Due to the conversion of hydroquinone and p-benzoquinone, hydroquinone has attracted the attention of researchers in the field of supercapacitors. David Vonlanthen et al. constructed a stable polyaniline-benzoquinone-hydroquinone supercapacitor and proved that the combination of conventional porous polyaniline and quinone electrolyte can improve electrochemical performance. The researchers combined two redox systems: polyaniline as the porous electrochemically active material and benzoquinone-hydroquinone redox pair as the electrolyte. Due to their small size and excellent electrochemical reversibility at low pH values, quinones are particularly suitable for use as redox active electrolytes, making them compatible with the acid-doped polymer family [33]. Singh et al. through simple shaking, hydroquinone can be physically adsorbed in the pores of activated carbon, and the material can be used in supercapacitors, with a specific capacitance of up to 200 Fg^{-1} in 1 M H_2SO_4 electrolyte. Due to the reversible redox chemistry of the hydroquinone/benzoquinone pair, nearly 40% of the specific capacitance is essentially pseudocapacitance, in which hydroquinone undergoes proton-coupled electron transfer to form benzoquinone [34].

The related literature on the redox mechanism of hydroquinone has given a clear explanation [35, 36]. However, because hydroquinone is an organic molecule, poor conductivity and cycle performance hinder its application. The large specific surface area of graphene can provide an ideal host environment for small hydroquinone particles. In the electrochemical reaction process, graphene and carbon nanotubes provide electric double-layer capacitance, and hydroquinone provides a larger pseudocapacitance in the process of gaining and losing electrons. Good progress has been made regarding the application of hydroquinone in the field of energy storage. Aditi Barua et al. clarified the role of temperature in a redox supercapacitor composed of nanoporous carbon@hydroquinone. At a high temperature of 50 °C, the nanoporous carbon@hydroquinone system shows the highest specific capacitance of 319 Fg^{-1}, which drops to 213 Fg^{-1} at a temperature of 10 °C. At the same time, when the temperature rises at both potentials, the charge transfer and double-layer capacitance are improved. The cycle stability at room temperature and 50 °C high temperature is 92% after 10,000 cycles and 86% after 5000 cycles, respectively, thus

showing the excellent stability of the nanoporous carbon@ hydroquinone system [37].

Studies have found that hydroquinone can also be compounded with conductive polymers to form a new structure to obtain good electrochemical performance [30]. Furthermore, hydroquinone can also be added to the electrolyte to improve the electrochemical performance of supercapacitors [38, 39]. At the same time, hydroquinone also has its shortcomings. It has poor electrical conductivity and poor cycling performance as a supercapacitor material. This article attempts to load HQ small molecules on the three-dimensional structure of rGO/CNTs to form a new three-dimensional electrode material. First, modified Hummers was used to prepare GO, the CNTs were subjected to reflux acidification treatment, and oxalic acid was used as a reducing agent to prepare rGO/CNTs/HQ hydrogels by a one-step low-temperature hydrothermal method. In the experimental process of GO forming a hydrogel, the π bond in the small molecule of HQ will recombine with the large π bond on the surface under the action of π-π. In the electrochemical test process, rGO and CNTs provide the composite material with electric double-layer capacitance, and HQ provides the pseudocapacitance.

Results and discussion

Figure 1 is a schematic diagram of the synthesis of rGO/CNTs/HQ hydrogel. The synthesis mechanism is: GO becomes locally hydrophobic due to its restored conjugation domain and reduced oxidation function after oxalic acid and hydrothermal reduction. Hydrophobicity and π-π interaction together lead to gelation between graphene sheets. During the hydrothermal reaction, the π bond in the hydroquinone molecule will be compounded with the large π bond on the surface of rGO due to the π-π interaction. At the same time, CNTs play the role of spacer and support in rGO/CNTs/HQ, which can effectively avoid the aggregation of GO during gel formation and improve the conductivity of rGO/CNTs/HQ.

Figure 2a and b is the actual picture of the rGO/CNTs/HQ hydrogel obtained in the experiment. It can be seen that the hydrogel was successfully prepared. The washed hydrogels all exhibited a cylindrical shape with the same shape as the vial, which indicates that the self-assembled hydrogels prepared after dehydration and condensation have a good
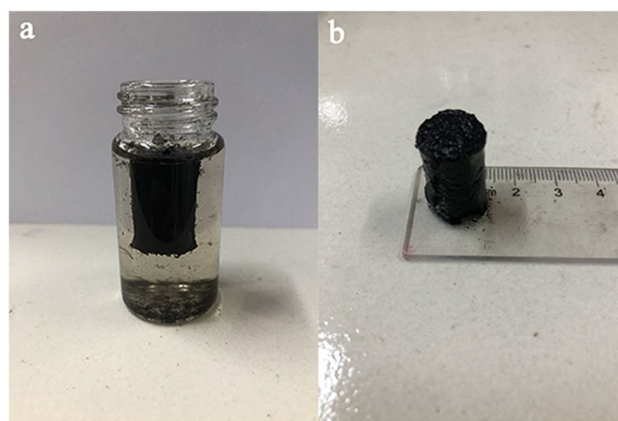

**Fig. 2 a,b** Physical image of rGO/CNTs/HQ

structure. Hydroquinone is covalently bonded to graphene to form a hydrogel structure with graphene and carbon nanotubes.

The XRD diffractometer is used to test the crystal structure of the sample. Figure 3a shows the XRD patterns of rGO/CNTs and rGO/CNTs/HQ. The intensity and peak shape of the diffraction peaks in the XRD pattern are a major criterion for distinguishing the crystallinity of composite materials. rGO/CNTs/HQ has two strong diffraction peaks at $2\theta = 25.8°$ and $2\theta = 43.0°$. The characteristic diffraction peak at $2\theta = 25.8°$ corresponds to the (002) crystal plane of the graphite structure. The half-width of the strong diffraction peak of rGO/CNTs/HQ at 25.8° is narrower than that of rGO/CNTs. According to the Scherrer formula, the particle size of rGO/CNTs/HQ composites has been reduced.

Figure 3b shows the Raman spectra of rGO/CNTs and rGO/CNTs/HQ. The D band is caused by some amorphous phases in the carbon ring of the graphene structure or the fracture of sp2 carbon bonds (the appearance of cleavage bonds and sp3 carbon bonds at the edges of graphene agglomerates). The G band is due to the sp2 carbon bond in the dense hexagonal graphene structure. In Fig. 3b, consistent with the previous, the peaks of rGO/CNTs at 1344 cm^{-1} and 1582 cm^{-1} are D peak and G peak, respectively. The D peak of rGO/CNTs/HQ hydrogel composite material appeared at 1344 cm^{-1}, and the G peak appeared at 1579 cm^{-1}. By calculation, the ID/IG values of rGO/CNTs and rGO/CNTs/HQ are 1.21 and 1.25, respectively. The ID/IG value of rGO/CNTs/HQ has become larger, indicating

**Fig. 1** Synthetic schematic diagram of rGO/CNTs/HQ
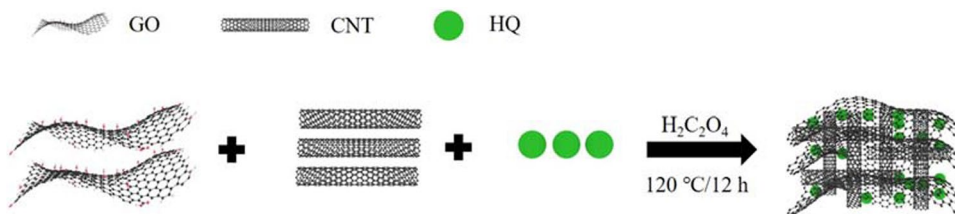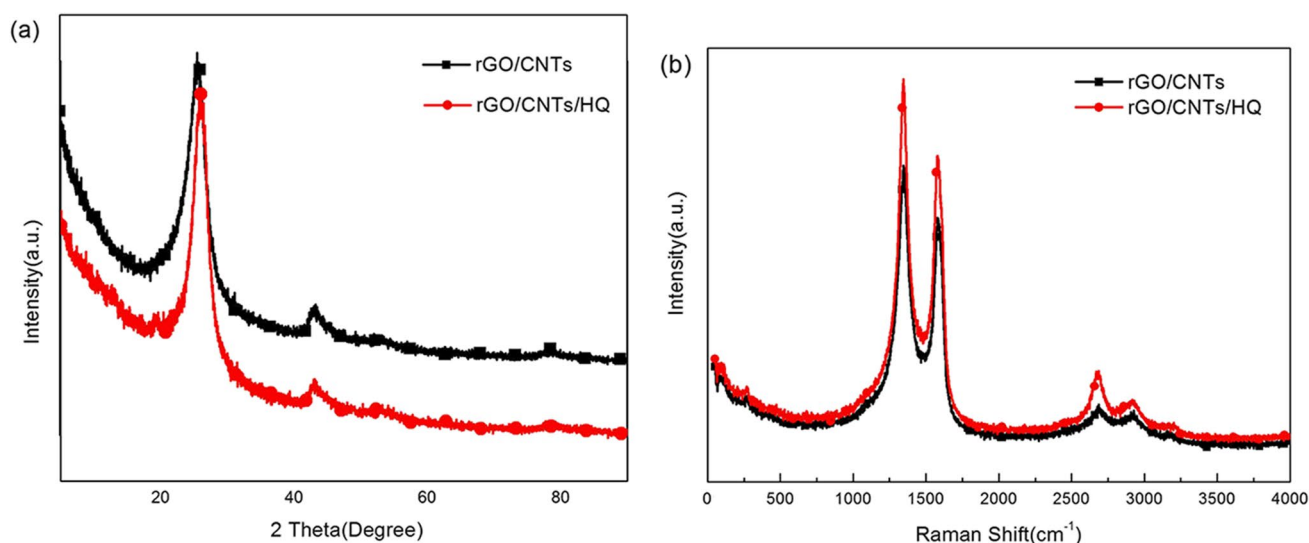
Fig. 3 **a** XRD patterns of rGO/CNTs and rGO/CNTs/HQ, **b** Raman spectra of rGO/CNTs and rGO/CNTs/HQ

that the composite graphene-based material has more defects after hydroquinone is compounded. At the same time, 2D bands appear at 2700 cm^{-1}, which is a characteristic of the graphene structure.

Figure 4 is the XPS spectrum of rGO/CNTs/HQ hydrogel, which is used to analyze the surface element composition of the material. The XPS full spectrum in Fig. 4a clearly shows the characteristic spectra of O 1 s and C 1 s, and Fig. 4b

illustrates the C 1 s spectrum of rGO/CNTs/HQ. It can be seen from the figure that the positions of the four peaks are 284.55, 285.11, 286.29, 289.35 eV and C=C/C-C, C-OH, C-O, C=O one-to-one correspondence; the strong peak at 284.55 eV represents the C atom arrangement of C=C bond. The peak at 285.11 eV is the C–OH bond, which makes the composite material have good wettability in the aqueous electrolyte. The peak at 286.29 eV is C-O, and the peak at

Fig. 4 XPS spectrum of rGO/CNTs/HQ: **a** full spectrum, **b** C 1 s, **c** O 1 s spectrum
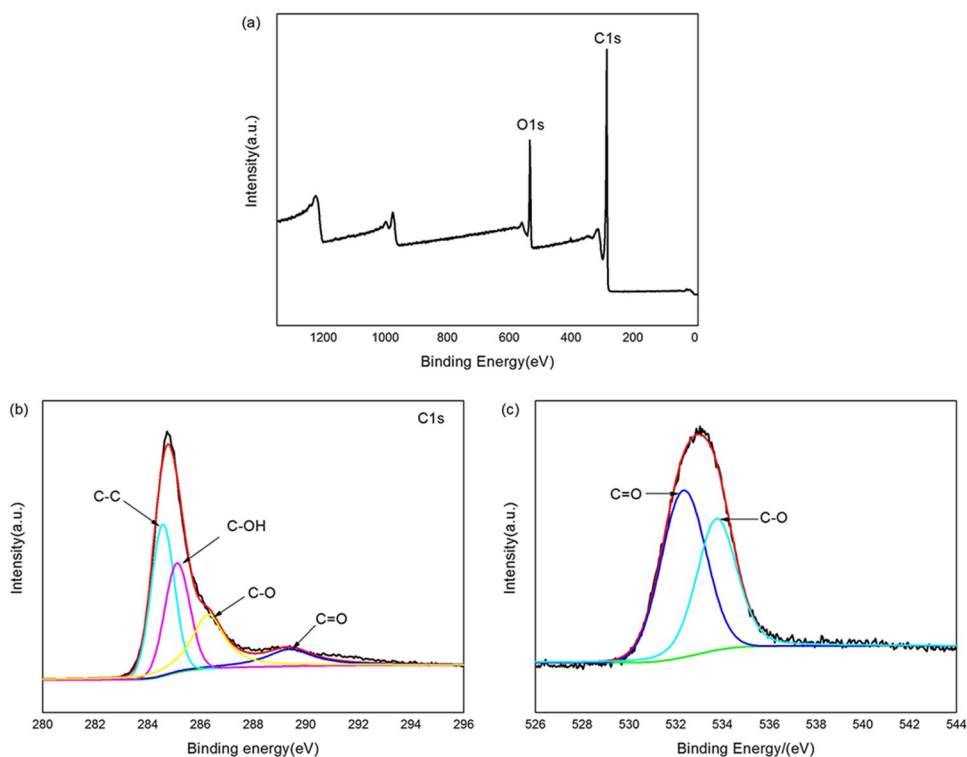
289.35 eV is C=O. The two indicate the difference in bond structure. The C 1 s XPS spectrum is basically consistent with the previous peak positions of rGO/CNTs. The O 1 s in Fig. 4c can be divided into two peaks. Compared with the pure rGO/CNTs, there is a deviation of about 3 eV. The strong peak at 532.33 eV and the strong peak at 533.73 eV may correspond to each other. For the oxygen bonds of C–O–R (ether) and O=C–O–R (ester), the O 1 s spectrum shows that the following experimental process occurred during the reaction experiment of forming hydrogel composites: First, the reaction is that HQ small molecules are oxidized to p-benzoquinone on the surface of GO. Then, the oxidation group on GO as a nucleophile is connected to p-benzoquinone, and the hydroxyl and carboxylic acid groups in GO are converted into ether bonds and ester bonds [40].

Figure 5a and b is the TEM image of rGO/CNTs/HQ hydrogel. The figure shows that the composite material has a lot of curls and wrinkles. It is precisely because these curls and wrinkles provide the hydrogel composite with a large available specific surface area. At the same time, the carbon nanotubes are interspersed to provide more conductive paths for the composite material, which inhibits the aggregation of the composite and improves the conductivity of the material, so that the electric double layer capacitance of the material can be improved. At the same time, this structure also provides a channel for the transmission of H^+, so that H^+ can fully diffuse into the composite material during the constant current charging and discharging process, which greatly improves the pseudocapacitance of the composite material.

Figure 6a and b are SEM images of rGO/CNTs/HQ hydrogel. It can be seen that the composite material presents a petal-like dispersion, which greatly increases the available specific surface area and provides more conductive paths for ion transmission. The carbon nanotubes play a supporting role in it. Space and promote electron transfer and other functions. The structure of Fig. 6b is different from that of Fig. 6a, indicating that the composite material has a variety of structures, and the lamella structure of rGO can also be seen.

In order to better compare and show the electrochemical performance, rGO/CNTs and rGO/CNTs/HQ were simultaneously prepared under the same experimental conditions, and both were tested; at the same time, the pure HQ samples were also tested under the same conditions, electrochemical testing. Figure 7 shows the CV curves of HQ, rGO/CNTs, and rGO/CNTs/HQ at 10, 20, and 50 mVs^{-1}. Under different scanning rates, the curve shapes of the three have no obvious changes, which proves that they all have good electrochemical stability in the electrochemical window. Obvious redox peaks appear on the CV curves of HQ and rGO/CNTs/HQ, but the CV curve area of HQ is much smaller than that of rGO/CNTs and rGO/CNTs/HQ, showing very poor capacitance characteristics. After the scan rate gradually increased to 50 mVs^{-1}, the area of the CV also increased simultaneously, and at the same time the oxidation peak and the reduction peak also moved to both sides. The oxidation peak and reduction peak on the CV curve of rGO/CNTs/HQ did not disappear, which confirmed that rGO/CNTs/HQ has excellent

Fig. 5 a,b TEM image of rGO/CNTs/HQ
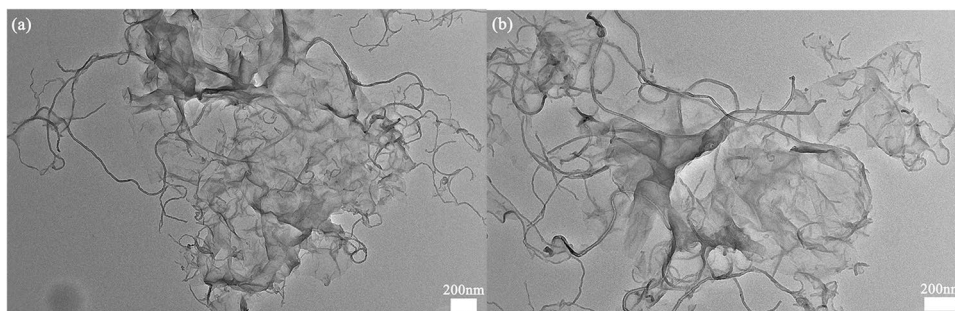
**Fig. 6 a,b** SEM image of rGO/CNTs/HQ
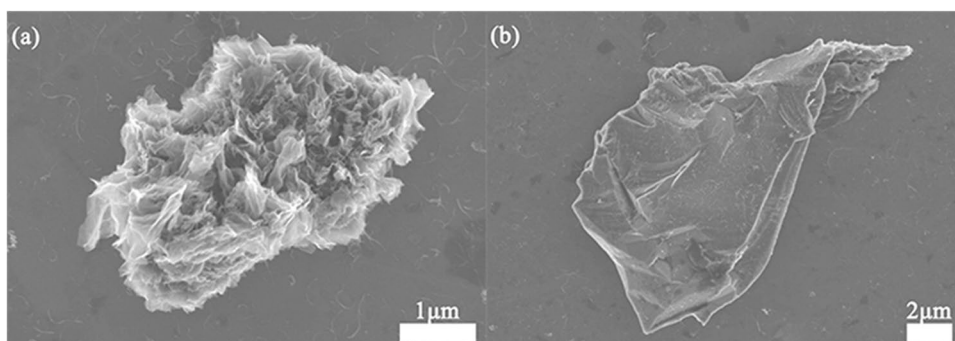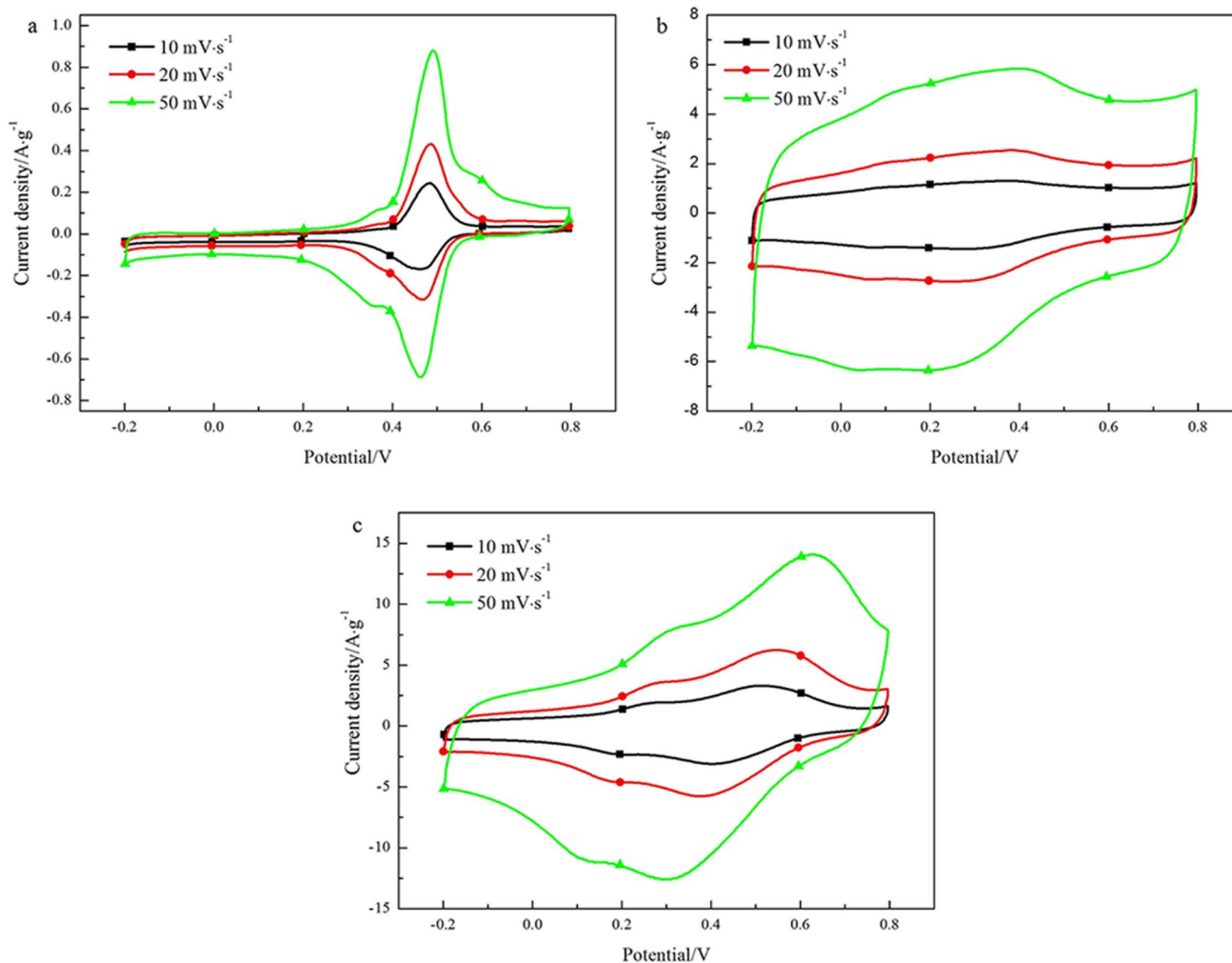
Fig. 7 CV curve of **a** HQ, **b** rGO/CNTs, **c** rGO/CNTs/HQ at different scan rates

pseudocapacitance characteristics and excellent reaction reversibility.

Figure 8 shows the GCD curves of HQ, rGO/CNTs and rGO/CNTs/HQ at 0.5, 1, 2, 5, and 10 A g^{-1}. A very obvious plateau appears on the GCD curve of HQ, indicating that it can provide pseudocapacitance; but at the same time, it can also be seen that the charging and discharging time of HQ is very short, and its energy storage properties are very poor. The GCD curves of rGO/CNTs and rGO/CNTs/HQ are similar to the triangle shape, and the charging and discharging time is long, indicating that both have excellent capacitance characteristics. However, since rGO/CNTs/HQ undergoes a redox reaction to provide pseudocapacitance, it can be seen that the GCD of rGO/CNTs/HQ is not linear, indicating that there is a plateau period, which corresponds to the CV test result. And rGO/CNTs/HQ has the longest charging and discharging time, indicating that it has the most excellent energy storage properties.

Figure 9a is the CV curve of HQ, rGO/CNTs, and rGO/CNTs/HQ at 10 mVs^{-1}. The figure shows that the CV curve area of HQ is very small, and it does not have capacitive performance. The CV curve of rGO/CNTs hydrogel is similar to a rectangle. The small peak may be due to a small amount of redox reaction in the small amount of oxygen-containing group of rGO. The main specific capacitance comes from the electric double layer capacitance. In addition to the electric double layer capacitance, the rGO/CNTs/HQ hydrogel also has two pairs of reversible redox peaks. The positions of these two pairs of reversible redox peaks are basically the same as the GCD curve of HQ, which provides a good pseudo capacitance. The large redox peak produced by the CV curve near 0.5 V is due to the electron transfer caused by the conversion of hydroquinone and hydroquinone. The redox peak near 0.2 V is caused by the covalent bonding of hydroquinone molecules with the oxidation groups on the surface of GO [39]. These two pairs of redox peaks provide a
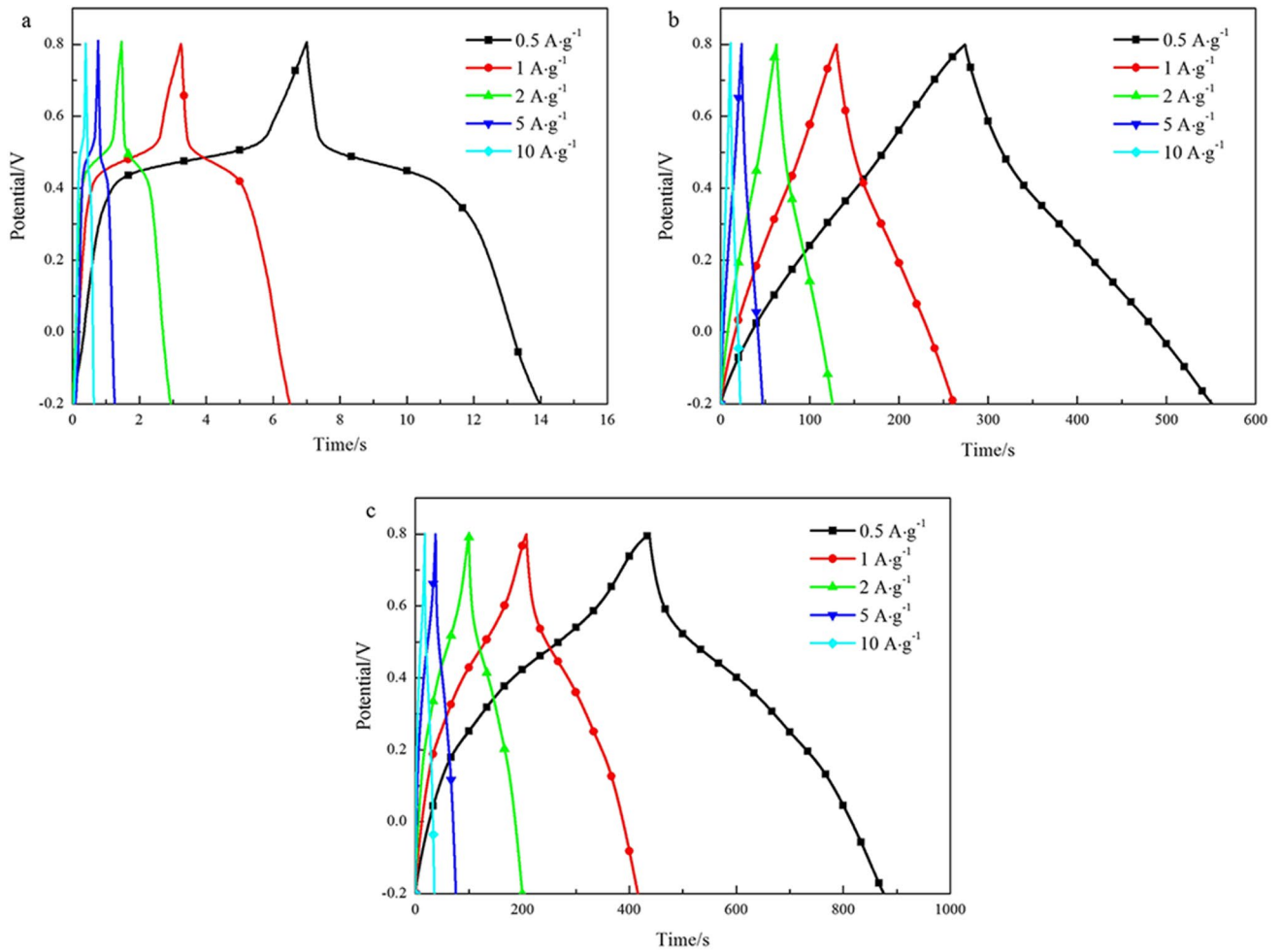
Fig. 8 GCD curve of **a** HQ, **b** rGO/CNTs, **c** rGO/CNTs/HQ at different current densities
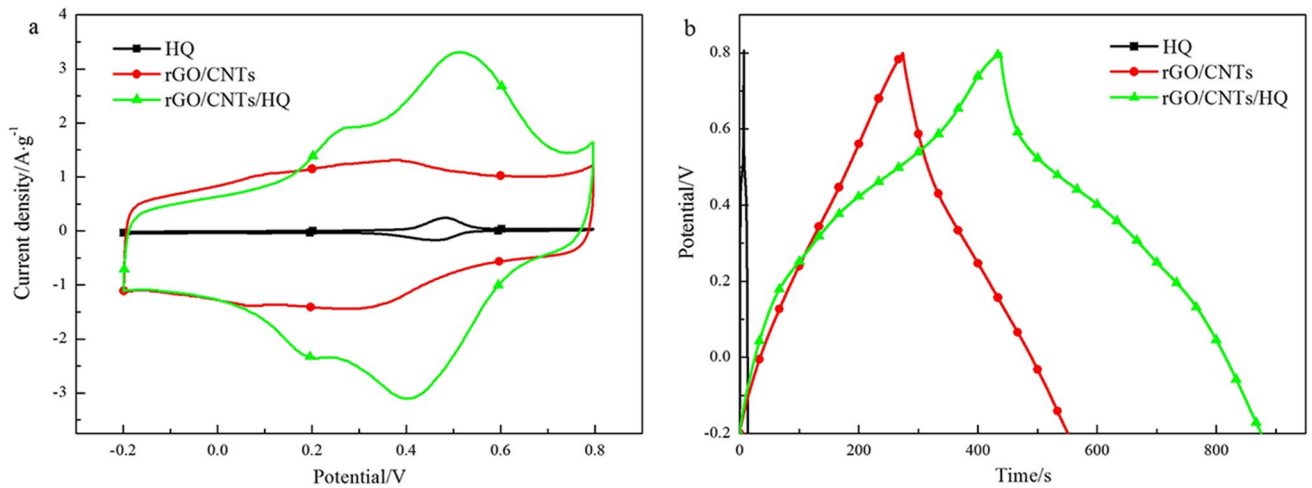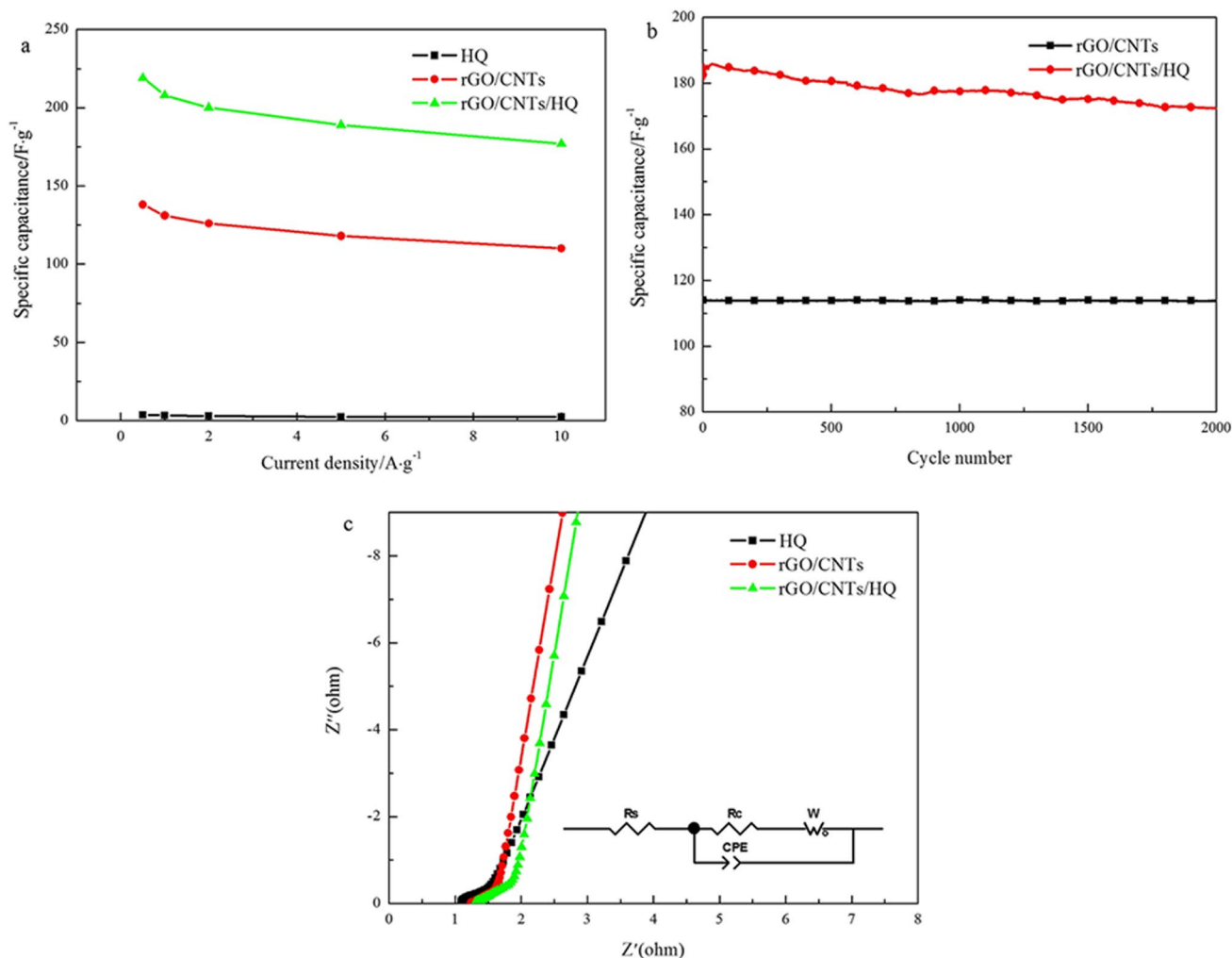

Fig. 9 **a** CV curve of HQ, rGO/CNTs, and rGO/CNTs/HQ at 5 mVs^{-1}, **b** GCD curve of HQ, rGO/CNTs, and rGO/CNTs/HQ at 0.5 Ag^{-1}

larger specific capacitance for the rGO/CNTs/HQ hydrogel. Figure 9b is the GCD curve of HQ, rGO/CNTs, and rGO/CNTs/HQ in the case of 0.5 Ag^{-1}. At 0.5 Ag^{-1}, the specific capacitance of rGO/CNTs/HQ hydrogel is 219 Fg^{-1}, which is much higher than the 138 Fg^{-1} of rGO/CNTs. It exhibits excellent electrochemical performance, while HQ is only 3.5 Fg^{-1} at 0.5 Ag^{-1}, which alone has poor energy storage properties as an electrode material, which corresponds to the CV curve.

Figure 10a shows that when rGO/CNTs and rGO/CNTs/HQ are at 0.5, 1, 2, 5, and 10 Ag^{-1}, the specific capacitances of rGO/CNTs/HQ are 219, 208, 200, 189, and 177 Fg^{-1}, respectively, and the specific capacitance of rGO/CNTs is 138, 131, 126, 118, and 110 Fg^{-1}, and for HQ, the capacitance value it can provide is negligible. From the above data, it can be seen that the mass-specific capacitance of rGO/CNTs is greatly improved after hydroquinone is compounded. When it is at 10 Ag^{-1}, rGO/CNTs/HQ still has a

specific capacitance of 177 Fg^{-1}. Compared with 0.5 Ag^{-1}, the specific capacitance can still retain 81% while preparing at the same time. The specific capacitance of rGO/CNTs can retain 80%, which proves that rGO/CNTs/HQ has excellent rate performance. Graphene has its shortcomings. The chemical inertness on its surface makes it impossible to overcome the van der Waals forces between the various layers. Therefore, it is inevitable that graphene has poor dispersion and relatively easy agglomeration during the use of graphene. The special size of carbon nanotubes can effectively inhibit the accumulation of graphene sheets during the interaction, and graphene can prevent the carbon nanotubes from entanglement. At the same time, the coiled six-membered ring structure of carbon nanotubes makes them easy to combine with graphene sheets through π-π interactions. Combining the two through self-assembly can effectively prevent the accumulation of graphene sheets, and the presence of carbon nanotubes will build a three-dimensional interconnected

Fig. 10 **a** Specific capacitance of HQ, rGO/CNTs, and rGO/CNTs/HQ at different current densities, **b** charge and discharge cycle diagram of rGO/CNTs and rGO/CNTs/HQ at 5 Ag^{-1}, **c** Nyquist plot and equivalent circuit diagram of HQ, rGO/CNTs, and rGO/CNTs/HQ

conductive network. In composite materials, graphene and carbon nanotubes provide electric double layer capacitance, while hydroquinone provides large pseudocapacitance. The main reasons for the excellent electrochemical performance of rGO/CNTs/HQ are as follows: First, rGO provides a sufficiently large available surface area for hydroquinone molecules, which can give full play to the advantages of pseudocapacitance. Secondly, all HQ molecules are directly attached to the rGO sheet through π-π interactions. This close contact makes full use of the pseudocapacitance component and provides fast electron transfer from rGO to HQ for the Faraday reaction. Finally, the intercalation of CNTs in each rGO layer provides more conductive paths for the composite material, reduces the internal resistance of the material, and expands the available specific surface area.

For practical applications of supercapacitors containing pseudocapacitors, the cycle performance must also be considered. Figure 10b shows the cycle performance graph of rGO/CNTs and rGO/CNTs/HQ at 5 Ag^{-1}. After 2,000 cycles, the specific capacitance of rGO/CNTs did not attenuate, while rGO/CNTs/HQ was slightly attenuated due to the composite HQ, retaining 94%, showing good cycle stability, indicating that HQ and HQ The non-covalent interaction between rGO is sufficient to maintain a long cycle life.

Figure 10c is the AC impedance diagram and equivalent circuit diagram of HQ, rGO/CNTs and rGO/CNTs/HQ. In the high frequency range, the HQ semicircle has the largest diameter, indicating that it has the largest charge transfer resistance when used alone as an electrode material, and the intercept between HQ and the horizontal axis is the smallest, indicating that its solution internal resistance is the smallest. In the low frequency range, the slopes of the curves of rGO/CNTs and rGO/CNTs/HQ are basically the same, indicating that the two have equivalent ion diffusion resistance, and HQ has the largest ion diffusion resistance. The electrochemical impedance spectroscopy shows that the resistance of the rGO/CNTs/HQ electrode system is increased compared to rGO/CNTs after the HQ small molecules are combined, but the resistance value is still very small, which is helpful for charge transfer and ion diffusion. However, HQ alone has the largest resistance overall and is not suitable for use as an electrode material alone.

Conclusions

In this paper, a simple one-step hydrothermal method is used to prepare rGO/CNTs/HQ hydrogels by incorporating HQ into the rGO/CNTs framework as a pseudocapacitance component through π-π interaction. The three-dimensional structure formed by rGO and CNTs can not only provide enough load space for the pseudocapacitance HQ molecules, but also can carry out rapid charge transfer between the three,

so that the rGO/CNTs/HQ hydrogel can achieve rapid ion diffusion and electrons transmission. The prepared rGO/CNTs/HQ has a mass-specific capacitance of 219 Fg^{-1} at 0.5 Ag^{-1}; at 10 Ag^{-1}, the mass-specific capacitance retains 81%, which has outstanding rate performance; After 2000 cycles of charging and discharging, the specific capacitance retains 94%, and it has good cycle performance. These electrochemical test results show that by carefully combining the surface functionalization and layered structure of graphene sheets, electrode materials with excellent performance can be obtained. Under the synergy of the three, rGO/CNTs/HQ is a potential supercapacitor electrode material.

Experimental section

Graphene pretreatment

GO was prepared from graphite crowd using a modified Hummers method [41].

Acidification of CNTs

To synthesize acidified CNTs, 30 ml H_2SO_4 and 10 ml HNO_3 were added into a three-necked bottle and heated at 140 ℃ for 2 h with stirring. After cooling down to room temperature, the carbon was washed with distilled water and ethanol. The prepared CNTs were dried in air at 60 ℃ for 12 h.

Preparation of rGO/CNTs hydrogel

To synthesize rGO/CNTs hydrogel, 20 mg GO, 20 mg CNTs, and 200 mg oxalic acid were added into 20 ml deionized water. The mixture was sonicated for 2 h and magnetic stirring for another 0.5 h. Finally, the mixed solution was transformed into a 20-ml glass bottle. The glass bottle was transformed into Teflon-lined stainless steel autoclave and heated at 120 ℃ for 12 h. After cooling down to room temperature, the black precipitate was washed with distilled water and ethanol.

Preparation of rGO/CNTs/HQ hydrogel

Twenty mg of GO, 20 mg of acidified CNTs, and 100 mg of oxalic acid were added to 20 mL of deionized water. The resulting solution was subjected to ultrasonic dispersion treatment for 1 h. Then 100 mg of hydroquinone was added to it, and then ultrasonic dispersion was carried out for 30 min. Stir for 30 min after sonication. After completion of the above treatment, the solution was placed in a glass vial, the opening of the glass vial was put into the reaction kettle, and the temperature was kept in a constant temperature

drying oven at 120 °C for 12 h. After the end, the sample was cleaned several times and placed in a constant temperature drying oven at 60 °C for 12 h. At the same time, rGO/CNTs hydrogels were prepared under the same experimental conditions and used as a control group for electrochemical testing.

Characterization

X-ray diffraction (XRD) patterns were carried out on X'Pert Pro MPD with a Cu Ka radiation source ($\lambda = 1.54056$ Å) worked at 40 kV. Raman spectroscopy (Raman) was observed using a 532 nm argument laser. Besides, the X-ray photoelectricity spectroscopy (XPS) was acquired by escalab250xi. The morphology and structure of materials were collected by scanning electron microscope (SEM, su8020), transmission electron microscope (TEM, JEM-2100f), and high-resolution transmission electron microscope (HRTEM, Jem-2100f).

Electrochemical test

The manufacturing process of the working electrode was described as follows: weigh the active material, acetylene black, and PVDF, respectively, according to the proportion of 8:1:1, mix them evenly, add 1-methyl-2-pyrrolidone, grind them fully to form a uniform slurry, then smear the slurry on the platinum mesh electrode, dry them at 60 °C for 12 h, and the mass of the active material was about 2 mg. All the electrochemical tests were carried out in the three-electrode system by using the electrochemical workstation cs310, in which the platinum mesh electrode coated with active substances, the platinum sheet electrode, and the saturated calomel electrode were corresponding to the working electrode, counter electrode, and reference electrode, respectively, and the electrolyte was HCL solution with the concentration of 1 mol/L. The electrochemical properties of the electrode materials were tested by cyclic voltammetry (CV), galvanostatic charge–discharge (GCD), and electrochemical impedance spectroscopy (EIS).

References

1. Yang P, Mai W (2014) Flexible solid-state electrochemical supercapacitors[J]. Nano Energy 8:274–290
2. Zhai Z-B, Huang K-J, Wu X, Hu H, Xu Y, Chai R-M (2019) Metal-organic framework derived small sized metal sulfide nanoparticles anchored on N-doped carbon plates for high-capacity energy storage. Dalton Trans 48(14):4712–4718
3. Zhai Z-B, Huang K-J, Wu X (2018) Superior mixed Co-Cd selenide nanorods for high performance alkaline battery-supercapacitor hybrid energy storage. Nano Energy 47:89–95
4. Xing L-L, Huang K-J, Cao S-X, Pang H (2018) Chestnut shell-like $Li_4Ti_5O_{12}$ hollow spheres for high-performance aqueous asymmetric supercapacitors. Chem Eng J 332:253–259
5. Wu X, Zhang H, Zhai Z-B, Xu J, Huang K-J (2020) Tellurium-impregnated P-doped porous carbon nanosheets as both cathode and anode for an ultrastable hybrid aqueous energy storage. J Mater Chem A 8(33):17185–17192
6. Llx A, Xu WB, Kjh A (2018) High-performance supercapacitor based on three-dimensional flower-shaped $Li_4Ti_5O_{12}$-graphene hybrid and pine needles derived honeycomb carbon - ScienceDirect[J]. J Colloid Interface Sci 529:171–179
7. Wu X, Zhai Z-B, Huang K-J, Ren R-R, Wang F (2020) Boosting energy and power performance of aqueous energy storage by engineering ultra-fine metallic VSe_2 nanoparticles anchored reduced graphene oxide. J Power Sources, 448
8. Sial QA, Javed MS, Lee Y-J, Le TD, Seo H (2020) Flexible and transparent graphene-based supercapacitors decorated with nanohybrid of tungsten oxide nanoflakes and nitrogen-doped-graphene quantum dots[J]. Ceram Int 46(14):23145–23154
9. Zhang L, Cai P, Wei Z, Liu T, Yu J, Al-Ghamdi AA et al (2021) Synthesis of reduced graphene oxide supported nickel-cobalt-layered double hydroxide nanosheets for supercapacitors[J]. J Colloid Interface Sci 588:637–645
10. Liu Y, Xin N, Yang Q, Shi W (2021) 3D CNTs/graphene network conductive substrate supported MOFs-derived CoZn-NiS nanosheet arrays for ultra-high volumetric/gravimetric energy density hybrid supercapacitor[J]. J Colloid Interface Sci 583:288–298
11. Gayathri S, Arunkumar P, Han JH (2021) Scanty graphene-driven phase control and heteroatom functionalization of ZIF-67-derived CoP-draped N-doped carbon/graphene as a hybrid electrode for high-performance asymmetric supercapacitor[J]. J Colloid Interface Sci 582:1136–1148
12. Quoc BL, Haojie F, Bubulinca C, Ngwabebhoh FA, Kazantseva NE, Saha P (2020) Reduced graphene oxide composited with Ni-MOF and PANI applied as electrodes for supercapacitor[J]. ECS Trans 99(1):93–101
13. Andikaey Z, Ensafi AA, Rezaei B (2020) Synthesis of engineered graphene nanocomposites coated with NiCo metal-organic frameworks as electrodes for high-quality supercapacitor[J]. Int J Hydrogen Energy 45(56):32059–32071
14. Makkar P, Ghosh NN (2021) High-performance all-solid-state flexible asymmetric supercapacitor device based on a Ag-Ni nanoparticle-decorated reduced graphene oxide nanocomposite as an advanced cathode material[J]. Ind Eng Chem Res 60(4):1666–1674
15. Xia H, Ragavendran KR, Xie J, Lu L (2012) Ultrafine $LiMn_2O_4$/carbon nanotube nanocomposite with excellent rate capability and cycling stability for lithium-ion batteries[J]. J Power Sources 212:28–34
16. Jia X, Yan C, Chen Z, Wang R, Zhang Q, Guo L et al (2011) Direct growth of flexible $LiMn_2O_4$/CNT lithium-ion cathodes[J]. Chem Commun 47(34):9669–9671
17. Sandhiya M, Balaji SS, Sathish M (2020) Boosting the energy density of flexible supercapacitors by redox-additive hydrogels[J]. Energy Fuels 34(9):11536–11546
18. Cong H-P, Ren X-C, Wang P, Yu S-H (2012) Macroscopic multifunctional graphene-based hydrogels and aerogels by a metal ion induced self-assembly process[J]. ACS Nano 6(3):2693–2703
19. Kabiri S, Tran DNH, Altalhi T, Losic D (2014) Outstanding adsorption performance of graphene-carbon nanotube aerogels for continuous oil removal[J]. Carbon 80:523–533

20. Kumar GG, Hashmi S, Karthikeyan C, GhavamiNejad A, Vatankhah-Varnoosfaderani M, Stadler FJ (2014) Graphene oxide/carbon nanotube composite hydrogels-versatile materials for microbial fuel cell applications[J]. Macromol Rapid Commun 35(21):1861–1865

21. Hashmi S, GhavamiNejad A, Obiweluozor FO, Vatankhah-Varnoosfaderani M, Stadler FJ (2012) Supramolecular interaction controlled diffusion mechanism and improved mechanical behavior of hybrid hydrogel systems of Zwitterions and CNT[J]. Macromolecules 45(24):9804–9815

22. Compton OC, Nguyen ST (2010) Graphene oxide, highly reduced graphene oxide, and graphene: versatile building blocks for carbon-based materials[J]. Small 6(6):711–723

23. Chen, Hamon, Hu, Chen, Rao, Eklund et al (1998) Solution properties of single-walled carbon nanotubes[J]. Science (New York, N.Y.), 282 (5386): 95–98

24. O'Connell MJ, Boul P, Ericson LM, Huffman C, Yuhuang W, Haroz E et al (2001) Reversible water-solubilization of single-walled carbon nanotubes by polymer wrapping[J]. Chem Phys Lett 342(3–4):265–271

25. Tung VC, Chen L-M, Allen MJ, Wassei JK, Nelson K, Kaner RB et al (2009) Low-temperature solution processing of graphene-carbon nanotube hybrid materials for high-performance transparent conductors[J]. Nano Lett 9(5):1949–1955

26. Zhang M, Gao B, Cao X, Yang L (2013) Synthesis of a multifunctional graphene-carbon nanotube aerogel and its strong adsorption of lead from aqueous solution[J]. RSC Adv 3(43):21099–21105

27. Dong X, Chen J, Ma Y, Wang J, Chan-Park MB, Liu X et al (2012) Superhydrophobic and superoleophilic hybrid foam of graphene and carbon nanotube for selective removal of oils or organic solvents from the surface of water[J]. Chem Commun 48(86):10660–10662

28. Qiu Z, He D, Wang Y, Li J (2017) Low-temperature fabrication of 3D drilled graphene sheets hydrogel for supercapacitors with ultralong cycle life[J]. Chem Phys Lett 684:290–297

29. Gao X-L, Wang D-D, Li S, Xing W, Yan Z-F (2018) Hydroquinone-modified mesoporous carbon nanospheres with excellent capacitive performance[J]. J Inorg Mater 33(1):48–52

30. Ren L, Zhang G, Lei J, Wang Y, Hu D (2018) Novel layered polyaniline-poly(hydroquinone)/graphene film as supercapacitor electrode with enhanced rate performance and cycling stability[J]. J Colloid Interface Sci 512:300–307

31. Sun Q, He T, Li Y (2020) A novel all solid-state asymmetric supercapacitor with superior electrochemical performance in a wide temperature range using a hydroquinone modified graphene xerogel as the cathode and N-doped Ti3C2Tx as the anode[J]. J Mater Chem A 8(4):1687–1696

32. Han C, Ye Y, Wang G, Hong W, Feng C (2018) Selective electro-oxidation of phenol to benzoquinone/hydroquinone on polyaniline enhances capacitance and cycling stability of polyaniline electrodes[J]. Chem Eng J 347:648–659

33. Vonlanthen D, Lazarev P, See KA, Wudl F, Heeger AJ (2014) A STab polyaniline-benzoquinone-hydroquinone supercapacitor[J]. Adv Mater 26(30):5095–5100

34. Singh C, Paul A (2015) Physisorbed hydroquinone on activated charcoal as a supercapacitor: an application of proton-coupled electron transfer[J]. J Phys Chem C 119(21):11382–11390

35. Park J, Kumar V, Wang X, Lee PS, Kim W (2017) Investigation of charge transfer kinetics at carbon/hydroquinone interfaces for redox-active-electrolyte supercapacitors[J]. ACS Appl Mater Interfaces 9(39):33728–33734

36. Zhang ZJ, Chen XY (2018) Illustrating the effect of electron withdrawing and electron donating groups adherent to p-hydroquinone on supercapacitor performance: the cases of sulfonic acid and methoxyl groups[J]. Electrochim Acta 282:563–574

37. Barua A, Paul A (2020) Unravelling the role of temperature in a redox supercapacitor composed of multifarious nanoporous carbon@hydroquinone[J]. RSC Adv 10(3):1799–1810

38. Xie H, Zhu Y, Wu Y, Wu Z, Liu E (2014) The effect of hydroquinone as an electrolyte additive on electrochemical performance of the polyaniline supercapacitor[J]. Mater Res Bull 50:303–306

39. Chen Y-C, Lin L-Y (2019) Investigating the redox behavior of activated carbon supercapacitors with hydroquinone and p-phenylenediamine dual redox additives in the electrolyte[J]. J Colloid Interf Sci 537:295–305

40. Jokar E, Shahrokhian S, Zad AI (2014) Electrochemical functionalization of graphene nanosheets with catechol derivatives as an effective method for preparation of highly performance supercapacitors[J]. Electrochim Acta 147:136–142

41. Chen C, Yu C, Fu X, Wang Z (2014) Synthesis of graphite oxide-wrapped CuO nanocomposites for electrocatalytic oxidation of glucose[J]. Synth React Inorg, Met-Org, Nano-Met Chem 44(10):1521–1525